Review of Scientific Instruments

Dynamic analysis of a Rayleigh scattering setup using synthetic light signals from a modulated LED

Cite as: Rev. Sci. Instrum. **90**, 063109 (2019); https://doi.org/10.1063/1.5112802
Submitted: 15 January 2019 . Accepted: 02 June 2019 . Published Online: 24 June 2019

Bertrand Mercier, and Thomas Castelain

Review of Scientific Instruments ARTICLE scitation.org/journal/rsi

Dynamic analysis of a Rayleigh scattering setup using synthetic light signals from a modulated LED

Cite as: Rev. Sci. Instrum. 90, 063109 (2019); doi: 10.1063/1.5112802
Submitted: 15 January 2019 • Accepted: 2 June 2019 •
Published Online: 24 June 2019

Bertrand Mercier[1,a] and Thomas Castelain[2]

AFFILIATIONS

[1] Univ Lyon, École Centrale de Lyon, INSA Lyon, Université Claude Bernard Lyon I, CNRS, LMFA, UMR 5509, 36 Avenue Guy de Collongue, F-69134 Ecully, France

[2] Univ Lyon, Université Claude Bernard Lyon I, École Centrale de Lyon, INSA Lyon, CNRS, LMFA, UMR5509, 43 Boulevard du 11 Novembre 1918, F-69100 Villeurbanne, France

[a] b.h.mercier@tudelft.nl

ABSTRACT

Rayleigh scattering of a laser beam can be used for time-resolved local measurements of density in flows. A key-point of the approach lies in extracting flow density statistics from the measurement of the scattered-light power. Complex hardware equipment and software procedures are involved in this process. The present paper offers a method to assess the entire chain of acquisition of a typical setup in realistic conditions, and an analysis of its dynamic performances with respect to the theoretical expectations. This is achieved by simulating the light intensity fluctuations typically observed with a Rayleigh scattering setup, by use of a known light intensity fluctuation signal generated using a light-emitting diode modulated in output power. The tested Rayleigh scattering setup is shown to perfectly satisfy the theoretical predictions, meaning that it allows us to measure the spectrum of light intensity variations with an outstanding linearity within a dynamic range proportional to the square-root of the measurement time.

I. INTRODUCTION

In the context of experimental fluid mechanics, the local flow properties must be measured by keeping the smallest impact of the probing system on the flow. Optical methods are therefore well suited for such an objective. Methods based on the light scattered by the molecules constituting the flow itself are the least intrusive methods. Contrary to the methods requiring tracers like particles[2,13] that involve inertia lag, or fluorescing molecules[12] that slightly change the chemical flow composition, molecular scattering based methods maintain all flow properties unchanged. Light scattering processes can be inelastic, which means that the scattered light wavelength differs from that of the incoming light, or elastic when the scattered light wavelength is unmodified. Elastic processes generally refer to Rayleigh and Mie scattering. The former rests upon the hypothesis of small scattering particles in comparison with the light wavelength; the latter is generalized to model all kinds of particles. Visible light scattered by molecules is here considered; the scattering process can hence be modeled by the Rayleigh scattering. This mechanism was already exploited for local density measurements in high Mach numbers flows[4] in the early eighties with a 5 mW laser as light source, and a photomultiplier to examine the scattered light. Later in the nineties, planar density measurement systems were developed with the pulsed laser as light source, and the CCD camera as sensor.[1,3] Insightful results were obtained, but planar measurements were limited to snapshot of the density fields and could not offer time resolved results due to the limited repetition rate of the pulsed lasers. This limitation can be thought to be partially circumvented by use of pulse burst laser systems that generate burst of high intensity pulses at a high repetition frequency, but only for a short time.[11] In parallel with planar development, pointwise density measurement systems based on a continuous-wave laser were perfected by Panda and Seasholtz. Those systems demonstrated a good ability for measuring time-averaged density[9] and time-resolved density fluctuations.[7,8,10]

The principle of density measurements based on Rayleigh scattering is described as follows. When a molecule is illuminated by the laser light pointing towards a unique direction, it scatters a small fraction of this incident light toward all directions. The ability of a given molecule to scatter light of a given wavelength, and in a given direction relative to the polarization plane of the incident light, is represented by its differential scattering cross section $\partial\sigma/\partial\Omega$. Therefore, a part of this light can be detected by a device covering a solid angle $d\Omega$. For an incident laser light of power I and an observed air volume of size V_{sc}, the power of light detected by the device P is proportional to the number of scatterers in the volume, thus to the number of molecules, and to the density ρ such that

$$P = Q_E V_{sc} \frac{\partial\sigma}{\partial\Omega} d\Omega I \frac{N_A}{\mathcal{M}} \rho, \tag{1}$$

where Q_E is the quantum efficiency of the detector equal to the ratio of the detected light power to the incoming light power, $\mathcal{M}$ is the molar mass, and N_A is the Avogadro constant. For a given experimental setup and a given gas or gas mixture, this relation implies that P is proportional to ρ; the experiment specific proportionality constant can be determined by the calibration methods previously described.[6] A typical order of magnitude of the constant obtained by the authors[6] is 10^{-11} W/(kg m^{-3}) with $V_{sc} \simeq 1$ mm^3 and a 5 W laser. A convenient method to measure such a small power is to consider the detected light as a flux of photons Φ given by

$$\Phi = P/E \tag{2}$$

with $E = hc/\lambda$ the energy of a photon, h the Planck constant, and c the speed of light. For $P = 10^{-11}$ W, $\Phi \simeq 10^7$ photons/s. In order to estimate the power of the detected light, the photon arrival rate can be determined by counting their detections. Photons are commonly detected by a photomultiplier tube.

In practice, in addition to the light coming from the probed volume, a small amount of stray light is also detected. The stray light is for instance induced by the laser reflections on the rig and is constant in time. Consequently, a flux Φ_0 is added to the Rayleigh scattering contribution leading to

$$\Phi = k\rho + \Phi_0, \tag{3}$$

where k is a constant of proportionality set by the abovementioned physical parameters.

Photon counting is performed by a dedicated system which exhibits some limitations. One limitation is caused by the minimum time delay required by the counter to count two individual photon detections, resulting in a maximum achievable counting rate. Another limitation is the maximum length of continuous records that is mostly related to the size of the counter buffer memory. A well know commercial counter is the SRS SR-400 with only 5 ns of minimum time delay between two counts, but the maximum recording time is short. On the contrary, the Hamamatsu C9744 allows for much longer records but with a minimum time delay of 25 ns. As it will be further justified in Sec. II B, an intrinsic uncertainty arises in signals obtained by photon-counting and requires a large counting rate to be overcome. Besides, to analyze the dynamic of a multiscale phenomenon such as those often observed in fluid mechanics, the record must be as long as possible, but commercial systems do not fit these two constrains. The authors therefore decided to setup a customized system based on a high speed data acquisition card that digitizes a photomultiplier output signal and allows us to perform the counting *a posteriori* using a software procedure. A validation of this setup is proposed in Mercier *et al.*[6] on the basis of data recorded in high speed jets. One aim of the present contribution is to introduce a new procedure that helps in determining the dynamic performances of the optical setup and whose use could be generalized to the characterization of any photon-counting device. This procedure consists in simulating light intensity variations to be observed from Rayleigh scattering measurements in flows holding density fluctuations by use of a light-emitting diode (LED) driven by a prescribed fluctuating current signal. Setting the spectrum properties of this input signal close to those of real density fluctuations allows for assessing the entire chain of acquisitions by comparing the output signal based on photon counting to the input driving signal.

In Sec. II, the experimental setup, and the photon counting procedure are described. This is followed by the analysis of the static and the dynamic responses of the LED. Then, the spectral properties of the signal derived from a hot-wire measurement of the velocity in a turbulent flow to simulate density fluctuations are presented. Finally, the ability of the chain of acquisition and of the data processing procedure, to recover the reference signal from the light intensity measurement are assessed.

II. METHODOLOGY

A. Setup description

The setup is arranged to allow the conversion of known electric signals into light intensity and the light intensity into a photon count-rate. A block diagram of the system is provided in Fig. 1. The first process is handled by a specially designed voltage-controlled LED driving unit which supplies a conventional 3 mm in diameter low power green gallium phosphide (GaP) LED with a current i. This current is determined from the input voltage $V_{in} = \overline{V_{in}} + V'_{in}$, where V'_{in} is the fluctuating voltage, controlled externally, and $\overline{V_{in}}$ is the average voltage set inside the driving unit. The current flowing through the LED is continuously monitored by the output V_{out}. More details about the driving unit are provided in Sec. II C. The LED is held behind a 1 mm pinhole in the field of view of a Hamamatsu H7422p-40 photomultiplier within a distance of 10 cm. This is a current output photomultiplier suited for photon counting applications due to its low rise time of 1 ns. At the peak wavelength of the LED, which is close to 570 nm, the quantum efficiency of the photomultiplier is approximately 40%. To prevent the ambient stray light

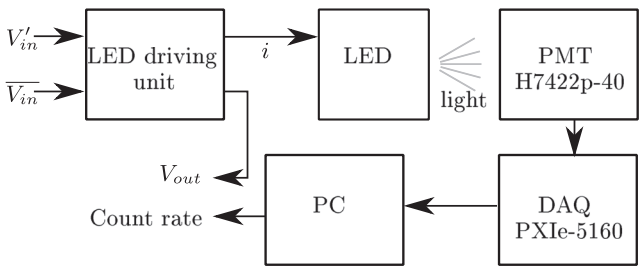

FIG. 1. Block diagram of the setup.

from biasing the measurements, the LED and the photomultiplier are placed in a dark box.

The output signal of the photomultiplier is digitized at a frequency of 1.25 GHz by a National Instrument PXIe-5160 and the photon counting operation is performed on the recorded digital signal.

B. Photon counting

Each photon detection by the H7422p-40 is converted into a burst of electrons at the photomultiplier output. It corresponds to a voltage pulse across the 50 Ω input impedance of the PXIe-5160 digitizer. The signal recorded during a run is therefore made of pulses corresponding to photon detections and of a low level background noise. An example of a signal obtained for a constant brightness of the LED is shown in Fig. 2. With such a signal, the background noise can be simply removed by considering only the peaks that are above a given threshold. The value of the threshold should be kept as low as possible to prevent missing photon detection signatures of low amplitude, but must be high enough to avoid counting any background noise as a detection. Once all peaks are identified, their times of arrivals are recorded in a table. A time history of the photon count rate $N_c(t)$ can then be obtained by counting all photons arrived during successive intervals of time. The width δt of these interval also define the sampling frequency $f_s = 1/\delta t$ of the photon count rate time history.

At this step, $N_c(t)/\delta t$ represents the number of counted photons per unit of time. However, as shown in Fig. 2, the delay between two photon detections is randomly distributed. Therefore, there is a probability for two photons to be detected within a very short delay. If the delay is shorter than a time constant τ called the pulse pair resolution, only one photon is counted. This time constant is related to the chain of acquisition, and its value is usually between 1 ns and 20 ns. Besides, the higher the count rate, the higher the probability for two detections to superimpose. This bias introduces a nonlinearity between $N_c(t)$ and $N(t)$, the unbiased value of the photons detection rate which is linearly related to the density.

It is, though, possible to recover the value of $N(t)$ from $N_c(t)$ by modeling the distribution of the delay between two detections using Poisson's statistics. The probability that n photons are detected during a time interval dt is

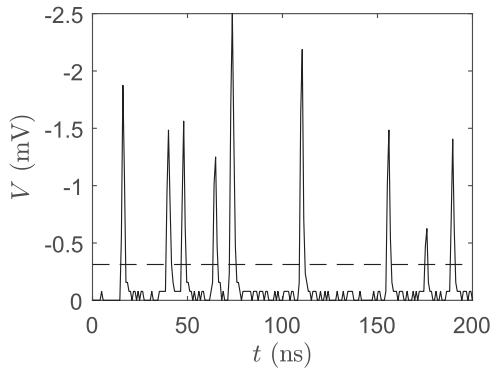

FIG. 2. Digitized photomultiplier output signal. The dashed line shows the threshold.

$$p(n, dt) = \frac{(\Phi dt)^n}{n!} e^{-dt\Phi}. \tag{4}$$

The probability that a photon is counted is equal to the probability that no photon is detected during the following time interval τ, that is, $p(0, \tau) = e^{-\tau\Phi}$. Consequently, the flux of counted photons is related to the flux of detected photon that is proportional to the density by

$$\Phi_c = \Phi e^{-\tau\Phi} \tag{5}$$

or, since $N_c = \Phi_c/f_s$ and $N = \Phi/f_s$,

$$N_c = N e^{-\tau N f_s}. \tag{6}$$

N is then obtained by inverting Eq. (6) using the Lambert-W function, or an approximated expression is[6]

$$N = \frac{N_c}{1 - \tau N_c f_s}. \tag{7}$$

The randomness of photon arrival leads to another difficulty. For a constant scattered power, a constant flux of photons is expected. However, when looking at Fig. 2, if a small interval of time is considered, say, 50 ns, it is clear that 3 photons are detected within $t = 0$ ns and $t = 50$ ns, while only one is detected between $t = 75$ ns and $t = 125$ ns. As a consequence, the measured flux of photons Φ_c can only be regarded if it is averaged during a long time. The values of N that are determined from N_c and Eq. (7) during much smaller time interval to allow high frequency analysis are therefore affected by the so-called *shot noise*. This noise follows Poisson's statistics, for which the variance of the noise $\mathrm{VAR}(N_{sn})$ is equal to the expected value $\overline{N}$. Thus, the standard deviation of $N_c(t)$ due to the shot noise N_{sn}^{rms} is

$$N_{sn}^{rms} = \sqrt{\overline{N(t)}}. \tag{8}$$

Moreover, the Poisson distribution can be well approximated by a white Gaussian distribution for $\overline{N}$ greater than 12.

C. LED driving unit

The role of the LED driving unit is to control the LED light intensity by applying an arbitrary electric signal at the input. Low current GaP LED light intensity is nearly linearly related to the current over a wide current range; see for instance the Vishay TLHG4605 LED datasheet. Consequently, the driving unit was designed as a voltage to current converter based on a low noise operational amplifier. The schematics of the driving unit are provided in Fig. 3. For a perfect operational amplifier, the voltage must be the same at the + and − pins of the circuit; therefore, the input voltage V_{in} is equal to the output voltage V_{out}. Since for a perfect amplifier, no current flows through pins + and −, the current flowing through the feedback branch is the same as that through the resistor R. Then, for the perfect operational amplifier,

$$i = \frac{V_{out}}{R} = \frac{V_{in}}{R}. \tag{9}$$

A capacitor C_c, chosen such that its impedance is much larger than the LED dynamic impedance $\mathrm{d}V/\mathrm{d}i$ below a few megahertz is installed to prevent high frequency oscillations. Consequently, the current flowing through the capacitor is negligible with respect to i in the range of frequency considered. The current i, also measured by

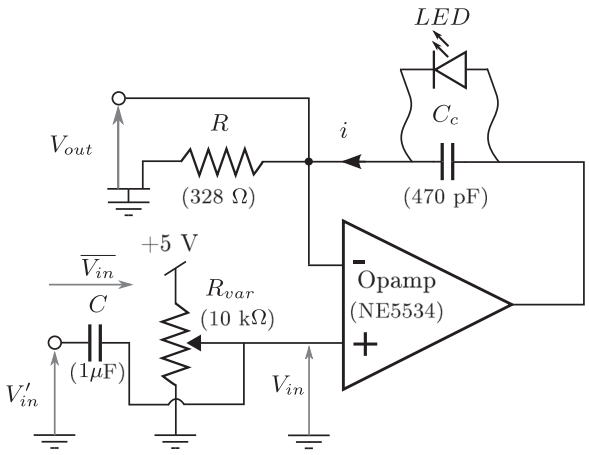

FIG. 3. Simplified schematic of the LED driving unit.

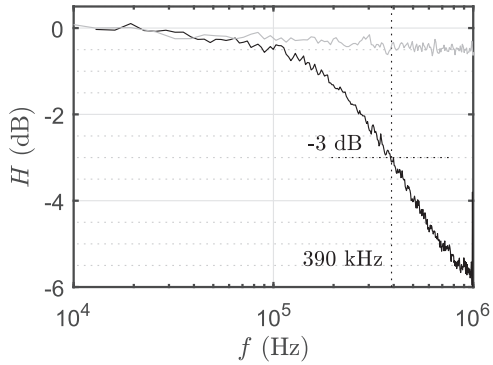

FIG. 5. Frequency response of the LED intensity in black and of the output current of the driving unit in gray.

the voltage drop across the resistor R, is thus also the current flowing across the LED.

D. Driving unit performances

The static performances of the system made of the driving unit and the LED are assessed by applying a series of constant input voltages V_{in} to the driving unit and by measuring simultaneously the time-averaged values of the output current i and the photon flux collected by the photomultiplier. The challenge resides in preventing the LED junction from heating-up when high currents are applied, which would reduce its efficiency and bias the results. This difficulty is worked around by reducing the measurement time at a given V_{in} and by repeating measurements to reduce the shot noise influence of the photon flux results. The evolution of $\overline{\Phi}_c$ and $\overline{\Phi}$ with $\overline{i}$ are provided in Fig. 4. The detected flux Φ is corrected from Φ_c by Eq. (7) with $\tau = 1.6$ ns as determined in a previous study.[6] The difference between these two quantities is caused by the pile-up effect briefly presented in Sec. II B and increases when the flux of photons rises, as expected. Although the light intensity of the LED rises very slowly with the current below $i = 4$ mA, a region where Φ increases linearly with i is observed between $i = 5$ mA and $i = 12$ mA. This linearity is comparable to that observed for density measurements, as stated in Eq. (3). As a consequence, from these measurements in static conditions, it can be concluded that as long as the current is kept within the linear region, variations of i, and thus, variations of the input V_{in}, can be used to simulate variations of flow density.

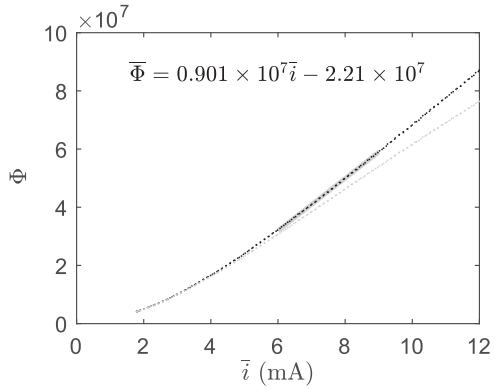

FIG. 4. Counted photon flux Φ_c (gray dotted curve) and detected photon flux Φ (black dotted curve) against the current i that flow through LED. The gray line shows the best fit in the linear region of the calibration curve.

Dynamic performances are evaluated by applying a sine sweep of frequency ranging from 10 kHz to 1 MHz to the driving unit input. The average current is set at 7.57 mA, and the sine amplitude is 2.00 mA. The frequency responses of the driving unit, and of the LED associated photon count rate are presented in Fig. 5. The response of the driving unit output current i is nearly flat with a loss of only −0.5 dB at 1 MHz. The response of the LED light intensity is measured by tracking the amplitude of the fluctuations of the collected flux of photons against the sweep frequency. The efficiency of the LED decreases with the frequency, with a −3 dB cut-off frequency of 390 kHz. However, the response of the LED is very close to that of the driving unit up to 100 kHz. Therefore, the bandwidth of the setup is [0 100 kHz].

These results show that the light intensity of the LED can be modulated by an input reference signal. It therefore allows for assessing the ability of the system to measure accurately any light intensity fluctuation in real applications. There are two constrains for the input signal with the present setup; the minimum driving voltage V_{in} is high enough for the current to be higher than 5 mA, and the frequency content of the signal is contained between DC and 100 kHz.

III. REFERENCE DENSITY-LIKE SIGNAL

On the basis of the abovementioned properties, the system is able to transpose arbitrary electric signals into light flux provided its maximum frequency does not exceed 100 kHz. For the validation of the chain of acquisition, and of the processing methods, this signal must be representative of a real local density time history. In particular, it must comply with the turbulence properties, as for instance an appropriate integral time scale. Ideally, the signal should

be related to the density in a compressible flow and obtained either numerically, experimentally, or analytically using synthetic turbulence models for instance. Nevertheless, the present study concerns the ability of the Rayleigh scattering setup to correctly resolve the input spectrum of light fluctuations. This aptitude is considered to be weakly dependent of the nature of the input as long as it correctly represents the physics of a turbulent process. Rather than a density signal, for this study, the chosen reference signal is a velocity signal extracted from a 120 s hot wire measurement in a turbulent boundary layer. In fact, both velocity and density signals are expected to feature similar characteristics of the turbulence. The normalized spectrum of this signal is presented in Fig. 6. It has a dynamic of approximately four decades between the frequencies normalized by the sampling frequency 10^{-3} and 0.5, which is convenient for assessing the dynamic of the Rayleigh scattering based measurement system.

This signal is uploaded into a Tektronix AFG3102 arbitrary signal generator from which it is possible to adjust the rms value and the frequency. The DC offset is set independently on the driving unit. According to the driving unit performances, and to the available memory of the AFG3102 which is only capable of storing 128 000 samples, the signal is generated with a sampling frequency of 102.4 kHz, leading to a Shannon frequency of 51.2 kHz and a duration of 1.25 s.

The DC current is set to produce the same flux of photons as the Rayleigh scattering produces for a constant density, in a classical experimental setup. For instance, previous calibrations performed by the authors[5,6] led to a typical photon flux $\Phi \simeq 4.0 \times 10^7 \rho$ photons/s. For $\overline{\rho} = 1.2$ kg/m^3, one obtains $\overline{\Phi} = 4.8 \times 10^7$ photons/s, corresponding to a current $\overline{i} = 7.80$ mA according to the calibration curve of Fig. 4. The rms value of the current fluctuations i'_{rms} is determined to match a realistic turbulent intensity here defined as $\mathcal{I} = \Phi'_{rms}/\overline{\Phi}$, giving

$$i'_{rms} = \frac{\mathcal{I}\overline{\Phi}}{0.90 \times 10^7}. \tag{10}$$

For a typical value of $\mathcal{I} = 5\%$, $i'_{rms} = 0.27$ mA.

These figures can of course be adapted to explore the response of any system in different experimental conditions, either for low photon fluxes involving a large shot noise contribution or large photon fluxes for which corrections of the pile-up effect are of primary importance.

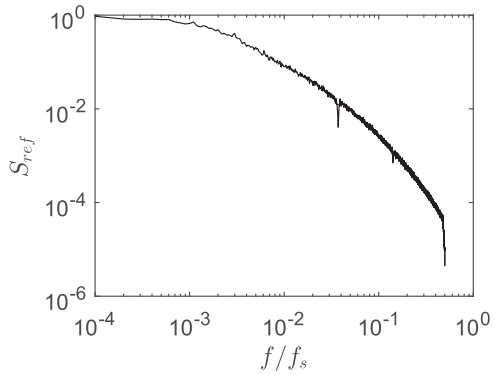

FIG. 6. Normalized spectrum of the reference signal for the LED intensity modulation.

IV. ESTIMATION OF THE FLUCTUATION SPECTRUM

A. Shot noise reduction method

In this section, we aim at estimating the spectrum of the current signal of features detailed in Sec. III. In any case, the signal of current is kept in the linear response region of the LED ensuring a similarity between the LED brightness and the light collected from a Rayleigh scattering process. Thus,

$$\Phi = ki + \Phi_0, \tag{11}$$

$$N = \frac{k}{f_s} i + \frac{\Phi_0}{f_s}. \tag{12}$$

The value of k is the slope of the linear region of the calibration curve in Fig. 4, and Φ_0 is the zero crossing flux of the fitting curve. Here, $k = 9.01 \times 10^6$ and $\Phi_0 = -2.21 \times 10^7$.

In most flows, the density fluctuations are small, and the shot noise is likely to be the strongest contribution to the photon count rate spectrum, and hence, to the LED current spectrum. Besides, the shot noise is a Poisson noise, thus a white noise. The level $P_{N_{sn}}$ of the shot noise contribution N_{sn}^{rms} in the count rate spectrum can therefore be determined easily from Parseval's identity since white noises have flat spectra. Indeed,

$$Var(N_{sn}) = \int_0^{f_s/2} P_{N_{sn}} df = P_{N_{sn}} \frac{f_s}{2} \tag{13}$$

and, from Poisson's law, $Var(N_{sn}) = \overline{N}$, and thus,

$$P_{N_{sn}} = \frac{2\overline{N}}{f_s}. \tag{14}$$

Furthermore, one has from Eq. (12),

$$\overline{N} = \frac{k\overline{i} + \Phi_0}{f_s} \tag{15}$$

and

$$N' = \frac{k}{f_s} i' \tag{16}$$

leading in terms of spectra to

$$P_{N_{sn}} = \frac{k^2}{f_s^2} P_{i_{sn}}. \tag{17}$$

By combining Eqs. (14), (15), and (17), the contribution of the shot noise in the LED current spectrum reads

$$P_{i_{sn}} = 2\frac{\overline{i} + \Phi_0/k}{k}. \tag{18}$$

The flow density $\overline{\rho}$, or the LED current $\overline{i}$ in this analogy, is in general imposed by the experiment. Therefore, the shot noise level in the density or current spectrum can only be reduced by increasing k. Yet, the value of k is upper bounded both by the pile-up effect and by the limits of the laser technologies.

Strategies to reduce the shot noise though exist. Panda and Seashlotz[10] proposed using two photomultipliers that probe

simultaneously the same volume. In Mercier *et al.*,[6] a method based on the same principle is provided, but instead of using two photomultipliers to obtain two signals, only one is used, and the count-rate time history is divided in two as follows: consider a signal $N_c(t)$ with $t = 0, dt, 2dt, 3dt, \ldots$, the first signal N_1 is made from the samples at $t = 2ndt$ with $n = 0, 1, 2, 3, \ldots$, and the second N_2 is made from the samples at $t = (2n + 1)dt$. Each signal is the sum of a coherent contribution, with the subscript s, representative of the physical signal to be characterized, and a noncoherent contribution associated with the shot noise, with the subscript sn. This gives

$$\begin{aligned} N_1 &= N_{1_s} + N_{1_{sn}}, \\ N_2 &= N_{2_s} + N_{2_{sn}}. \end{aligned} \tag{19}$$

These two signals are divided into m segments $N_1^i(t)$ and $N_2^i(t)$ with $i = 1, 2, 3, \ldots, m$ of time duration l_t determining the final frequency resolution Δf of the spectrum such that $\Delta f = 1/l_t$. Then, the cross-spectrum of the fluctuation $P_{N_1N_2}$ is obtained as follows:

$$P_{N_1N_2}(f) = \frac{2}{m}\sum_i^m F_{N_1^i}(f)F_{N_2^i}^*(f), \tag{20}$$

where F is the Fourier transform and * denotes the complex conjugate. Using the decomposition in Eq. (19),

$$\begin{aligned} P_{N_1N_2}(f) = \frac{2}{m}\sum_{i=1}^m & \underbrace{F_{N_{1_{sn}}^i} F_{N_{2_s}^i}^* + F_{N_{1_s}^i} F_{N_{2_{sn}}^i}^*}_{\text{(a)}} \\ & + \underbrace{F_{N_{1_{sn}}^i} F_{N_{2_{sn}}^i}^*}_{\text{(b)}} + \underbrace{F_{N_{1_s}^i} F_{N_{2_s}^i}^*}_{\text{(c)}}. \end{aligned} \tag{21}$$

Terms (a) and (b) involve the shot noise contributions $N_{1_{sn}}^i$ and $N_{2_{sn}}^i$ that are random and independent. Besides, their complex Fourier transform coefficients are also random and centered on zero. As a consequence, for large values of m, the contribution to the sum of terms (a) and (b) vanishes out. The term (c) only involves coherent contributions. Then,

$$\lim_{m\to\infty} |P_{N_1N_2}(f)| = \left|\frac{2}{m}\sum_{i=1}^m F_{N_{1_s}^i} F_{N_{2_s}^i}^*\right|. \tag{22}$$

Moreover, if the sampling frequency is high enough with respect to the frequency of the coherent fluctuations, N_{1_s} and N_{2_s} are expected to be strongly correlated, and only time shifted by a delay dt. Therefore, for large value of m, $P_{N_1N_2}(f)$ is a good approximation of the spectrum of the signal s

$$\lim_{m\to\infty} |P_{N_1N_2}(f)| \simeq |P_{N_{1_s}N_{1_s}}| \simeq |P_{N_{2_s}N_{2_s}}|. \tag{23}$$

Unfortunately, the number m of signal segments is limited and a residual contribution of the shot noise remains in the fluctuations. This corresponds to a noise floor in the spectra of value $P_{N_{res}}$. This noise floor is reached when the shot noise contribution is much larger than the coherent fluctuations. For that reason, terms (a) and (c) in Eq. (21) that involve coherent fluctuation are neglected compared to the term (b), and the residual noise floor $P_{N_{res}}$ is

$$P_{N_{res}} = \left|\frac{2}{m}\sum_{i=1}^m F_{N_{1_{sn}}^i} F_{N_{2_{sn}}^i}^*\right|. \tag{24}$$

The expected value of $P_{N_{res}}$ can be determined as a function of m by noting z_i the random complex number $z_i = e^{j\theta_i}$, where $j = \sqrt{-1}$, and θ_i is a random variable such that $F_{N_{1_{sn}}^i} F_{N_{2_{sn}}^i}^* = |F_{N_{1_{sn}}^i} F_{N_{2_{sn}}^i}^*| z_i$. Since N_1 and N_2 are both extracted from N by halving the sampling frequency, from Parseval's identity

$$|F_{N_{1_{sn}}^i} F_{N_{2_{sn}}^i}^*| = \frac{4\overline{N}}{f_s} = 2P_{N_{sn}}. \tag{25}$$

Equation (24) becomes

$$P_{N_{res}} = \frac{2P_{N_{sn}}}{m}\left|\sum_{i=1}^m z_i\right| = \frac{4\overline{N}}{mf_s}\left|\sum_{i=1}^m z_i\right|. \tag{26}$$

Noting that

$$\begin{aligned} |\sum_{i=1}^m z_i| &= \left(\sum_{i=1}^m z_i \sum_{j=1}^m z_j^*\right)^{1/2} \\ &= \left(\sum_{i=1}^m\sum_{j=1}^m \underbrace{z_i z_j^* \delta_{ij}}_{i=j} + \sum_{i=1}^m\sum_{j=1}^m \underbrace{z_i z_j^* (1-\delta_{ij})}_{i\neq j}\right)^{1/2} \end{aligned} \tag{27}$$

and that

$$\begin{aligned} \sum_{i=1}^m\sum_{j=1}^m z_i z_j^* \delta_{ij} &= m, \\ \lim_{m\to\infty}\sum_{i=1}^m\sum_{j=1}^m z_i z_j^* (1-\delta_{ij}) &= 0, \end{aligned} \tag{28}$$

we obtain

$$P_{N_{res}} = \frac{4}{\sqrt{m}}\frac{\overline{N}}{f_s} \tag{29}$$

similarly in this particular application,

$$P_{i_{res}} = \frac{4}{\sqrt{m}}\frac{\bar{i} + \Phi_0/k}{k}. \tag{30}$$

The residual noise floor emerging from the shot noise decreases with $\sqrt{m}$; large values of m are therefore required to reduce the noise floor by orders of magnitude. The number m of segments is set on one hand by the recording length, and on the other hand by the desired frequency resolution of the spectrum. Lower resolution (higher value of Δf) means more segments for the same recording time, and thus lower noise floor.

B. Validation

In this section, the decay of the level of the noise floor with the number of segments is verified and compared to the prediction in Eq. (30). Then, the effect on the spectra of the signal splitting needed for the shot noise reduction is analyzed.

The data set used in this section consists of 1170 independent records of 0.86 s each, this duration being the longest record achievable by the PXIe-5160 digitizer with the present configuration. The total length of the record is therefore a little longer than 1000 s. Each record is initially a photomultiplier output signal from which count rate time histories are extracted following the method provided in Sec. II B.

For the analysis of the noise floor decay, the sampling frequency f_s of the count rate time history $N(t)$ is chosen to be f_s = 409.6 kHz. With that f_s, the maximum frequency of the fluctuating current spectrum P_i is $f_s/4$ = 102.4 kHz. Besides, the signal generator used to generate V'_{in} at the LED driving unit input has a sampling frequency of 102.4 kHz. The maximum frequency of LED brightness fluctuation is therefore 51.2 kHz. Hence, the fluctuations measured on the spectrum P_i are only attributable to the residual noise floor within the range 51.2 kHz–102.4 kHz. As a consequence, the residual noise floor $P_{i_{res}}$ is estimated as the average value of P_i between 51.2 kHz and 102.4 kHz. The evolution of $P_{i_{res}}$ against m is displayed in Fig. 7. For the values of m between 2 and 1170 (which corresponds to the total number of independent recordings), the spectrum P_i is evaluated using m recordings; for the values of m greater than 1170, recordings are partitioned, and P_i is evaluated from the partitions. A maximum value of 344 partitions by recording is used, leading to the maximum value $m = 344 \times 1170 = 4 \times 10^5$. A very good agreement is found between the measured and the predicted values of $P_{i_{res}}$. For m below 5×10^4, the decay slope is −0.5 as expected. Above, $P_{i_{res}}$ slightly oscillates near the prediction. The model given in Eq. (30) to predict the shot noise level given the calibration parameters and the number of segment m is validated, and provides consistent predictions.

The analysis now focuses on the effect on spectra of splitting N into N_1 and N_2. To this purpose, spectra of the current fluctuations P_i are computed with N sampled at different frequencies. The sampling frequencies f_s = 409.6 kHz, f_s = 102.4 kHz, and f_s = 25.6 kHz are retained. The largest is well above the LED current fluctuations, while the smallest is similar with the high frequencies of i'.

The three spectra, each evaluated with a frequency resolution of 100 Hz, are shown in Fig. 8. The spectrum obtained from the direct current measurement through V_{out} is also plotted for the comparison. For the two lowest f_s cases, the spectrum points out a strong decay of the amplitude for frequencies approaching the highest spectrum frequency. This drop is expected and corresponds to the reducing point to point coherence for high frequencies. An error larger than 5% is observed at $0.08f_s$ for f_s = 25.6 kHz and $0.10f_s$ for f_s = 102.4 kHz. These frequencies depend upon the coherence of turbulence in the investigated flow, but the present signal was chosen to be representative for typical turbulent flow. To prevent spectra from being biased, it is therefore reasonable to choose a sampling frequency at least 10–12 times larger than the maximum frequency of interest for the study. The value of 12 might seem to be large, but it must be put together with the fact than even if there was no bias, the minimum sampling frequency would be 4 times the desired frequency. Hence, the sampling frequency should only be multiplied by 3 to suppress the bias.

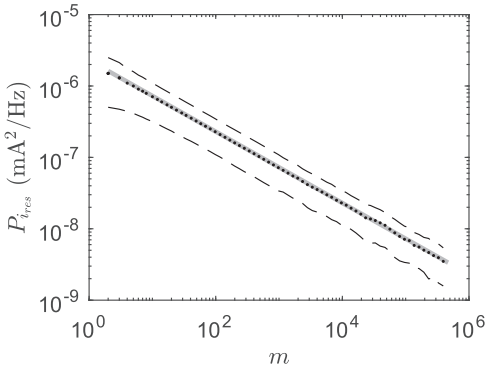

FIG. 7. Residual noise floor as a function of the number of segments used to compute the spectrum. Black dotted curve: measured value, gray solid curve: prediction from Eq. (30). Black dashed curve: ±1 standard deviation of the shot noise level.

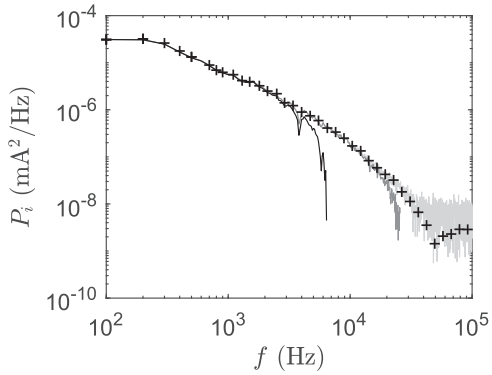

FIG. 8. Spectra for three different sampling frequencies. Light gray solid curve: f_s = 409.6 kHz, gray solid curve: f_s = 102.4 kHz, black solid curve: f_s = 25.6 kHz, and plus sign: reference measurement.

C. Practical spectra estimation with shot noise minimization

In practical estimations of density spectra from turbulent flows, the residual noise floor due to shot noise can prevent one from capturing the decay of turbulence level at a "high" frequency, typically above 1–10 kHz. On the other hand, flow field characterization often relies on a fine frequency resolution to capture possible resonances (e.g., cavity flows) or flow global instabilities (e.g., wake of bluff body flows), the signature of which are typically in the range of frequency 0.1–1 kHz at usual scales. These two constraints are not compatible as shown by Eq. (30): a low residual noise floor requires m to be large, and hence, a large frequency resolution also. A practical way to circumvent this feature is to estimate the spectrum of a given signal from the concatenation of portions of spectra computed with different frequency resolutions.

The result of such a procedure is illustrated in Fig. 9. This example is based on the same signal as that of Fig. 8, but analyzed using four different frequency resolutions: 20 Hz below 1 kHz, 100 Hz between 1 kHz and 10 kHz, 400 Hz between 10 kHz and 30 kHz, and 1600 Hz at frequencies above 30 kHz. The resulting spectrum indeed shows the main features of the original spectra while keeping the shot noise level below 10^{-8} A^2/Hz, allowing for a very good agreement between the measured spectrum from the fluctuations of LED light intensity and the reference current spectrum. In particular, low frequency features that were not visible in Fig. 8 with a frequency resolution of 100 Hz appear with the spectrum concatenation, whereas in the meantime, the shot noise level is lower in Fig. 9 than in Fig. 8.

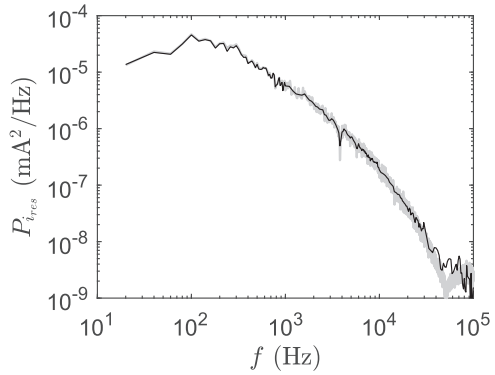

FIG. 9. Spectrum of the current fluctuations. Black solid curve: concatenated spectra, gray solid curve: reference spectrum.

V. CONCLUSION

A dynamic analysis of a Rayleigh scattering setup based on synthetic light signals is performed. Light signals are generated by a modulated LED fed by a dedicated driving unit, whose input corresponds to a sample of turbulent velocity signal. This system was found to allow for simulating the light fluctuations associated with a Rayleigh scattering process at frequencies up to 100 kHz.

The unit is designed to simultaneously measure the light intensity signal with the Rayleigh scattering setup and an electrical output signal that mimics the real light power emitted by the LED source. This allows for an effective comparison between the expected and the measured light signal characteristics, and, in particular, their spectral behaviors.

Spectra of the light signals measured by a photomultiplier, as used in classical Rayleigh scattering setups, are affected by the shot noise that imposes a residual noise floor, which limits the effective dynamic of the measurements. This noise floor can be reduced by applying a specific data processing to the signals. The procedure is however shown to introduce a bias that vanishes providing light signals are sampled at a frequency at least ten times larger than the maximum frequency of interest in the spectrum.

A model is derived to predict the performance of this data processing and is successfully compared to the experimental results. The model shows that the noise floor level is inversely proportional to the square root of the recording time, and to the square root of the frequency resolution. It therefore allows us to predict the minimum recording time needed to reach a desired noise floor level with a given frequency resolution. Conversely, for a given recording time, the proper frequency resolution for an appropriate shot noise level is provided by the model.

ACKNOWLEDGMENTS

This work was performed within the framework of the Labex CeLyA of Université de Lyon, within the program "Investissements d'Avenir" (Nos. ANR-10-LABX-0060/ANR-11-IDEX-0007) operated by the French National Research Agency (ANR), and is also partially supported by the industrial Chair ADOPSYS co-financed by SAFRAN-SNECMA and ANR (No. ANR-13-CHIN-0001-01).

REFERENCES

[1]N. J. Dam, M. Rodenburg, R. A. L. Tolboom, G. G. M. Stoffels, P. M. Huisman-Kleinherenbrink, and J. J. ter Meulen, "Imaging of an underexpanded nozzle flow by UV laser Rayleigh scattering," Exp. Fluids **24**(2), 93–101 (1998).

[2]N. Damaschke, V. Kühn, and H. Nobach, "A fair review of non-parametric bias-free autocorrelation and spectral methods for randomly sampled data in laser Doppler velocimetry," Digital Signal Process. **76**, 22–33 (2018).

[3]K. Fiedler, O. Sieber, and C. Jakiel, "Quantitative density measurements by Rayleigh scattering behind a plane turbine cascade," AIAA J. **35**(8), 1303–1308 (1997).

[4]P. Kreisler, W. Tietsch, and K. Bethge, "Measurement of the density of a gas jet by light scattering," Nucl. Instrum. Methods **177**(2-3), 521–527 (1980).

[5]B. Mercier, "Développement d'une méthode de mesure de la masse volumique par diffusion Rayleigh appliquée à l'étude du bruit de jets, et contribution à l'étude du screech dans les jets supersoniques sous détendus," Ph.D. thesis, 2017-LYSEC61, École Centrale de Lyon, 2017.

[6]B. Mercier, T. Castelain, E. Jondeau, and C. Bailly, "Density fluctuations measurement by Rayleigh scattering using a single photomultiplier," AIAA J. **56**(4), 1310–1316 (2017).

[7]J. Panda, "Two point space-time correlation of density fluctuations measured in high velocity free jets," AIAA Paper 2006-0006, 2006.

[8]J. Panda, "A molecular Rayleigh scattering setup to measure density fluctuations in thermal boundary layers," Exp. Fluids **57**(12), 183 (2016).

[9]J. Panda and R. Seasholtz, "Density measurement in underexpanded supersonic jets using Rayleigh scattering," AIAA Paper No. 98-281, 1998.

[10]J. Panda and R. G. Seasholtz, "Experimental investigation of density fluctuations in high-speed jets and correlation with generated noise," J. Fluid Mech. **450**, 97–130 (2002).

[11]M. J. Papageorge, C. Arndt, F. Fuest, W. Meier, and J. A. Sutton, "High-speed mixture fraction and temperature imaging of pulsed, turbulent fuel jets auto-igniting in high-temperature, vitiated co-flows," Exp. Fluids **55**(7), 1763 (2014).

[12]I. van Cruyningen, A. Lozano, and R. K. Hanson, "Quantitative imaging of concentration by planar laser-induced fluorescence," Exp. Fluids **10**(1), 41–49 (1990).

[13]J. Westerweel, G. E. Elsinga, and R. J. Adrian, "Particle image velocimetry for complex and turbulent flows," Annu. Rev. Fluid Mech. **45**(1), 409–436 (2013).